Criticality of the XY model in complex topologies

Miguel Ibáñez Berganza and Luca Leuzzi
IPCF-CNR, UOS Roma Kerberos.
Dipartimento di Fisica, Università "La Sapienza".
*Piazzale A. Moro, 5, 00185 Roma.**

The critical behavior of the $O(2)$ model on dilute Lévy graphs built on a 2D square lattice is analyzed. Different qualitative cases are probed, varying the exponent ρ governing the dependence on the distance of the connectivity probability distribution. The mean-field regime, as well as the long-range and short-range non-mean-field regimes are investigated by means of high-performance parallel Monte-Carlo numerical simulations running on GPU's. The relationship between the long-range ρ exponent and the effective dimension of an equivalent short-range system with the same critical behavior is investigated. Evidence is provided for the effective short-range dimension to coincide with the spectral dimension of the Lévy graph for the XY model.

I. INTRODUCTION: INTERACTING MODELS IN COMPLEX NETWORKS

The study of interacting systems defined in complex, non-regular structures is interesting from at least three points of view. Statistical mechanical models in graphs are used for the description of phenomena in different fields, among which one can cite: stock market dynamics,[1–4] correlations in bird flocking,[5] avalanches in brain activity[6] or biological networks.[7,8] Furthermore, there is a theoretical interest *per se* in the study of criticality in complex networks. The theory of critical phenomena establishes that the critical properties of systems interacting in a d-dimensional lattice only depend on the symmetries of the interaction and on the dimensionality d. On the other hand, when the topology of the interaction is more complicated, e.g., translational invariance is lost and symmetries of the lattice are broken, the dependence of criticality on the structural properties of the interacting graph is not known in general, although this topic has been subject of interest since more than two decades and several results are available for particular models.[9]

A particularly clear case is the spherical model, which has been proved to be equivalent to the $n \to \infty$ limit of the $O(n)$ model when both models are defined on a lattice.[10] On general graphs the full equivalence does not hold anymore, though the critical behavior of the spherical and $O(n \to \infty)$ still do coincide.[11] The critical properties of the spherical model on a general graph are exactly known[12] and are such that the universality class of the transition only depends on a single quantity: the spectral dimension of the graph, $\bar{d}$, defined in terms of the low-frequency spectral density of its adjacency matrix $\varrho(\omega) \sim \omega^{\bar{d}/2-1}$. This quantity is also related with the probability of self-return of a random walker in the graph, and determines the infrared divergences of a Gaussian field theory defined on the graph.[12,13] Remarkably, the functional dependence of the spherical model critical quantities on a graph with spectral dimension $\bar{d}$ turns out to be the same as the ones of a short-range model in a hyper-cubic lattice with Euclidean dimension $\bar{d}$. This analogy provides a suggestive, physical sense to the non-integer dimensions appearing in the context of the theory of critical phenomena.

The spectral dimension also plays a role in the XY model criticality, which was proved[14] to exhibit spontaneous magnetization in the ordered phase in a graph of spectral dimension $\bar{d} > 2$, and absence[15] of spontaneous magnetization for $\bar{d} \leq 2$. The latter phenomenon being well known in the two-dimensional (2D) XY model,[16–18] which is a particular case of this result.

Further numerical and analytical results for the criticality of other particular models in graphs are available (for a review see Ref. 9). The Ising model was first studied in Small-World networks,[19–23] in Barabasi-Albert networks,[23–25] and on general graphs,[26,27] where it was found that the universality class depends on the divergence or finiteness of the second and fourth moments of the degree distribution. In this way, three different critical regimes may be discriminated: (i) absence of phase transition, when both second and fourth moments diverge; (ii) a non-mean-field second order transition, when the second moment is finite; and (iii) a mean-field second-order transition, when both moments are finite.

Studies of the Ising model in scale-free networks[28] and in correlated growing-random networks[29,30] were also performed. In the latter case a phase transition was found of the Kosterlitz-Thouless (KT) universality class, different from the mean-field nature of the transition found in (uncorrelated) scale-free networks. This difference was argued to have its origin in the sign of the degree-degree correlations (assortativity-disassortativity) of both types of networks.[29,31] The Potts model has also been investigated,[32–34]finding an infinite-order transition for a divergent second moment of the degree distribution.

Eventually, also the $O(2)$ XY model has been analyzed. In the 1D Small-world network, it was argued[35] to exhibit long-range order for arbitrarily low values of the rewiring probability (like in the Ising case). For uncorrelated[4] and correlated[23] scale-free networks an order-disorder transition is observed for a sufficiently large value of the degree distribution exponent. Interestingly, as it happens in the Ising case, in the correlated scale-free network the transi-

tion is non-mean-field, unlike the uncorrelated case. This difference is again ascribed to the different nature of the degree-degree correlations in both kinds of graphs.[4]

Another piece of the puzzle is provided by the numerical work carried out by Yang *et al.*,[36] in which the critical behavior of the XY model is studied in uncorrelated and correlated *random* (rather than scale-free) graphs. In the first case, i.e., the Erdös-Rényi graph, the transition is found to be of the mean-field type, while in a randomly growing network it is claimed that the occurring transition belongs to the KT universality class.

Despite numerous results in this field, a unified picture of critical phenomena in graphs is still lacking. For instance, it is not clear under what conditions a relation can be established between criticality in graphs with spectral dimension $\bar{d}$ and short-range models in $\bar{d}$ dimensional lattices, nor what is the relation with the conjectured influence of dissasortativity on criticality.

Considering the field of disordered systems as well, spin-glass models defined in complex graphs have been recently investigated, on the so-called *Lévy* or *dilute* lattice[37] that we will use in the present work. It is a graph whose sites are connected with a probability decaying as a power ρ of the distance between them, as computed in a given, auxiliary, nearest-neighbor lattice. While for large enough ρ one recovers the auxiliary lattice, the $\rho = 0$ Lévy graph limit corresponds to the random Erdös-Rényi graph, such that the $zN/2$ bonds (z being the coordination number of the lattice) are chosen at random from the set of all $N(N-1)/2$ possible bonds. The Ising spin-glass model in the Lévy graph was introduced in Ref. 37 as a dilute variant of the fully connected Ising spin glass with long-range interactions in one dimension,[38–42] to allow for more efficient, i.e., $O[N]$ computation of observables in a graph with N sites. Like the fully connected long-range spin glass, the dilute one is such that, varying the power ρ, one actually acts as if varying the dimension of a D-dimensional short-range lattice model, equivalent –from the critical behavior point of view– to the long-range model.[37,42]

Starting from the field-theoretic representation in the free theory limit, valid both for ordered and disordered systems, an equivalence between ρ and D can be conjectured to be[37]

$$\begin{aligned} D &= \frac{2d}{\rho - d} \qquad \rho \in (d : 2 + d] \\ D &= d \qquad\qquad \rho \geq 2 + d \end{aligned} \tag{1}$$

where d is the dimension of the auxiliary lattice of the dilute model. This can be improved as[43]

$$D = \frac{(2 - \eta_{\rm sr})d}{\rho - d} \tag{2}$$

where $\eta_{\rm sr}$ is the anomalous scaling exponent of the space correlation function in the D-dimensional short-range counterpart. The above relationship does not depend on the specific symmetries of the system, nor on the presence of any long-range order at all (as in the quenched disordered case). What can change is the range of values of ρ determining the universality class at which the model belongs. In particular, for fully connected systems with (ordered or disordered) long range interactions decaying with the ρ-th power of the distance in a d-dimensional hyper-cubic lattice, three regimes can be identified:

- $d < \rho < \rho_{\rm mf}(d)$, in which the system undergoes a mean-field transition;
- $\rho_{\rm mf}(d) < \rho < 2 + d$, in which infra-red divergences take place, to be dealt with renormalization group;
- $\rho > 2 + d$ where the critical behavior is short-range-like.

d	Auxiliary lattice dim.
D	Critically equivalent short-range lattice dim.
$\bar{d}$	Lévy graph spectral dim.
$D_{\rm u}$	Upper critical dim.

TABLE I: Summary of the different dimensions considered.

The value of $\rho_{\rm mf}(d)$ depends on the specific theory and its symmetries, thus being different in ordered[44] ($\rho_{\rm mf} = 3d/2$) and disordered[39] ($\rho_{\rm mf} = 4d/3$) systems.

Critical exponents are functions of ρ as well, as, e.g., $\eta_\rho = 2 - \rho + d$ for any ρ (the η long-range exponent is not renormalized) and $\nu_\rho = 1/(\rho - d)$, in the mean-field regime. Also these expressions are formally the same both in ordered[44] and disordered[39,42] systems, whereas different is their dominion in ρ and the renormalized expression for $\rho > \rho_{\rm mf}(d)$. The prediction for the η_ρ exponent has been compared with the outcome of numerical simulations in the case of the long-range Ising ferromagnet.[45] On the other hand, Eq. (2) has been carefully tested in 1D Lévy Ising spin-glasses for $\rho > \rho_{\rm mf}(1) = 4/3$, verifying that the equivalent short-range critical behaviors are actually consistent both for $D = 3$ ($\rho = 1.792$) and for $D = 4$ ($\rho = 1.58$).[46]

To make reading more fluid and avoid notation ambiguities, in Tab. I we summarize the various dimensions we refer to in this work.

The possibility yielded by Lévy lattices of changing the effective dimensionality, freely choosing the universality class of the model without compromising the complexity, is useful to approach different problems: the applicability of the replica symmetry breaking theory in and out of the spin-glass mean-field regime,[37,47] the existence of the Almeida-Thouless critical line above the spin-glass upper critical dimension in Ising[48,49] and Heisenberg[50] systems, the criticality of the 3-spin spin glass,[43] and the low temperature behavior in Heisenberg spin-glasses (including the spin-chirality decoupling)[51,52] as well as in $O(m \to \infty)$ spin-glasses.[53]

There are some aspects that should be clarified also in this context. An elementary question is about the equivalence of the spectral dimension $\bar{d}$ of the graph and the

short-range equivalent dimension D, cf. Eq. (1). A rigorous derivation of the critical properties of long-range dilute models as a function of the power ρ is still lacking, and also an argument stating under what conditions they are equivalent to the fully connected case with the same value of the power ρ. In what follows we will clarify some of the mentioned issues in the $O(2)$ case defined in a dilute 2D graph with open and periodic boundary conditions. Along with theoretical arguments, we shall present the outcome of numerical simulations run on Graphics Processing Units (GPUs) with a *ad hoc* optimized code, whose dynamics is based on the Metropolis, Parallel Tempering and Over-relaxation algorithms, suited to study continuous spin models interacting in graphs with arbitrary topology.

The paper is organized as follows: in Sec. II we provide a theoretical argument to support the existence of three intervals of the power ρ, relative to three different universality classes of the $O(2)$ model defined on a dilute-2D graph with power ρ and we yield numerical evidence in support of the fact that $D(\rho)$ is, actually, the spectral dimension of the graph with power ρ. In Sec. III numerical methods are explained and the implementation of our GPU-based algorithm and its performance are reported. We present numerical results in Sec. IV and our conclusions in Sec. V.

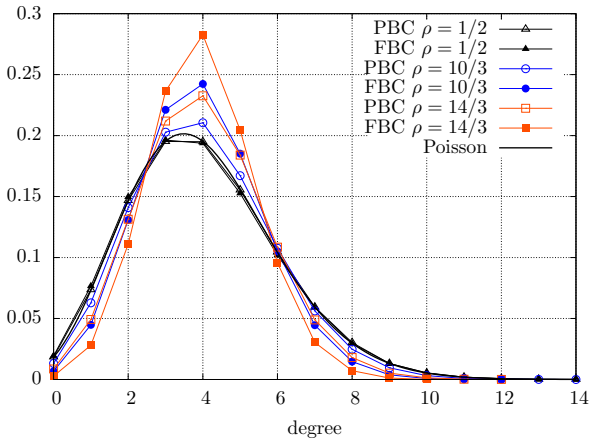

FIG. 1: Probability distribution of the degree of connectivity of dilute 2D graphs with $N = 256^2 = 2^{14}$ nodes for three values of the decay exponent $\rho = 1/2, 10/3$ and $14/3$ of the link probability, one for each critical regime. Results are reported for both periodic (open symbols) and free (closed symbols) boundary conditions. $\rho = 14/3$ is in the short-range regime, $\rho = 10/3$ in the non-mean-field regime and $\rho = 1/2$ in the mean-field regime. In the latter case the Poisson distribution with average 4 is displayed for comparison.

II. CRITICALITY OF THE XY MODEL IN THE 2D LÉVY GRAPH

We are concerned with the ferromagnetic $O(n)$ model, defined by the Hamiltonian:

$$H = -\sum_{i<j=1}^{N} J_{ij}\,\mathbf{S}_i \cdot \mathbf{S}_j, \tag{3}$$

where $\mathbf{S}_i$ denotes the dynamic variable on the i^{th} site of the graph, an n-dimensional vector with unit modulus, and the product is a n-dimensional Euclidean scalar product, the XY model being the $n = 2$ case. The values of the adjacency matrix J_{ij} of the graph can be either 0 (no connection) or 1 (the interaction strength). We will study the dilute (Lévy) graph, for which two sites i and j are connected (i.e., the element of the J_{ij} matrix is 1) with a probability

$$\begin{aligned} \mathcal{P}_\rho(J_{ij}) &= \frac{1}{Z}|\mathbf{r}_i - \mathbf{r}_j|^{-\rho} \\ Z &= \sum_r r^{-\rho} \end{aligned} \tag{4}$$

and such that the total number of bonds is independent from ρ and equal to $2N$. In Eq. (4), the vector $\mathbf{r}_i$ corresponds to the position of site i on a square lattice and the probability is normalized summing over the set of all possible distances between the sites of the 2D lattice. Operatively, the set of possible distances on lattices of linear size L depends on the boundary conditions chosen for the numerical simulation being periodic (PBC) or free (FBC). The maximum distance $r_{\max}$ will be $[L/2]\sqrt{2}$ for PBC or $L\sqrt{2}$ for FBC. In the present paper the results shown are for PBC, but the outcome of the numerical analysis presented in Sec.IV remains unchanged when FBC are implemented, despite the differences with graphs with PBC in the $\rho > 0$ case. In Fig. 1 we show the degree distribution of the dilute 2D graph (with free and PBC) for different values of ρ. While the $\rho \to \infty$ 2D limit of the Lévy graph (i.e., the square lattice) exhibits a delta function $\delta(\mathrm{d} - 4)$, the $\rho = 0$ limit corresponds to the Erdös-Rényi graph with degree distribution given by a Poisson distribution with average degree equal to 4. The latter case is independent from the kind of boundary conditions.

1. *A dimensional argument*

We now discuss the criticality of the model. Let us first consider the d-dimensional fully connected version of our model where each site is connected with any other site and the interaction strength decays with a power-law $J(\mathbf{r}) \sim |r|^{-\rho}$ of the distance in a d-dimensional lattice. Following Ref. 44, we consider the following effective Ginzburg-Landau Hamiltonian for the long-range model, a scalar ϕ^4 Sine-Gordon theory,

$$\mathcal{H} = L^d \int \frac{\mathrm{d}^d\mathbf{q}}{(2\pi)^d}\,(q^\psi + m^2)\,|\tilde{\phi}(\mathbf{q})|^2 + \frac{\lambda}{4!}\int \mathrm{d}^d\mathbf{r}\,\phi^4(\mathbf{r}) \tag{5}$$

where L is the linear size of the system, $\mathbf{q}$ is the momentum space index, m is the mass of the theory, $\tilde{\phi}$ is the Fourier Transform of the scalar field, and λ is the coupling strength. The long-range exponent ψ is such that the Fourier Transform of the interaction $J(\mathbf{r})$ goes like

$$\tilde{J}(q) = L^{-d/2} \int \mathrm{d}^d\mathbf{r}\, J(\mathbf{r}) e^{\imath \mathbf{r}\cdot\mathbf{q}} \sim q^{-\psi}$$

for low $q = |\mathbf{q}|$. In the long-range fully connected case ($J(\mathbf{r}) \sim r^{-\rho}$), it holds $\psi = \rho - d$, and there is a divergence for $\rho = d$, the point at which the number of links, proportional to $\tilde{J}(0)$, diverges in the thermodynamic limit.

A dimensional analysis of the Hamiltonian, Eq. (5), see, e.g., Refs. 37,39,42,44, shows that the dimension of the coupling constant λ is larger than zero whenever $\rho > 3d/2$. Below this point, λ is an irrelevant variable at criticality: the system critical behavior is correctly described by a (mean-field) free theory. For $\rho > 2 + d$, the short-range lattice contribution to the propagator, q^2, will take over the long-range q^ψ contribution and the Ginzburg-Landau Hamiltonian will correspond to the one of a d-dimensional short-range model. One cold argue that these arguments still remain valid in the case of the dilute Lévy lattice. We will motivate better in the following section such analogy (see also subsection II 2). Eventually, in the fully connected model, an ultra-extensive regime occurs for $\rho < d$, with diverging energy. This is not present in the dilute model, since the number of bonds of the graph is constant. Collecting all the above considerations, we summarize the following dependence of the criticality of the dilute XY model on the exponent ρ (see Fig. 2):

1. $\rho \geq \rho_{\rm sr} = 2 + d$: the model behaves as its short-range version in d dimensions, for what concerns criticality, thus belonging to the Kosterlitz-Thouless (KT) universality for $d = 2$. This regime will be called the *short-range regime* in the following.

2. $\rho \in (\rho_{\rm mf} : \rho_{\rm sr})$, with $\rho_{\rm mf} = 3d/2$: the system will present a transition different from a KT transition, with exponents different from the mean field-ones, this regime will be denoted as the *(long-range) non-mean field regime.*

3. $\rho \leq \rho_{\rm mf}$, the system belongs to the mean-field universality class, i.e., its critical properties are the corresponding to a free Gaussian theory in dimension 4. We will denote this regime as the *mean-field regime.*

2. Spectral dimension

Using Eq. (1), and naming $D_{\rm u}$ the upper critical dimension ($D_{\rm u} = 4$ for the present model) one checks that

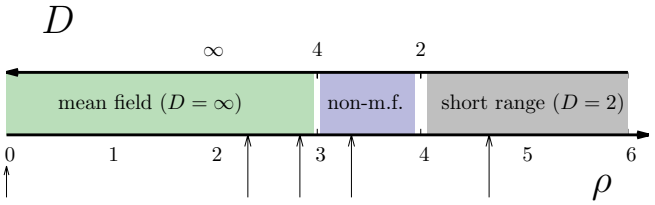

FIG. 2: Three domains of ρ, relative to the three universality classes of the dilute XY model on Lévy graph. The arrows point out at the values of ρ at which simulations have been carried out: $0, 14/6, 17/6, 20/6, 28/6$.

the regimes above introduced are in correspondence with the three regimes of an *equivalent* D-dimensional lattice model with nearest-neighbor interactions: (1) in the short-range regime, the critical behavior for the dilute model is as without the dilution: it is $D = d$; (2) in the non-mean-field regime it is $D \in (d : D_{\rm u})$ the system is not in the mean-field universality class; (3) in the mean-field regime, $D \geq D_{\rm u}$, the system is mean-field.

Remarkably, this comparison suggests the equality between D and the spectral dimension of the Lévy graph, $\bar{d}$. In Ref. 54 it is proved that a fully connected lattice with interaction strength decaying as $r^{-\rho}$ (r being the distance in a d-dimensional lattice) has spectral dimension:

$$\begin{aligned} \bar{d} &= d \qquad \text{if} \quad \rho > 2 + d \\ \bar{d} &= \frac{2d}{\rho - d} \qquad \text{if} \quad \rho \in (d : 2 + d] \end{aligned} \tag{6}$$

This would prove our conjecture about the three different critical regimes in the XY model provided that: *(a)* Eq. (6) holds for a Lévy lattice with power ρ, and that *(b)* the relationship between critical properties of a model on a graph with spectral dimension $\bar{d}$ and on a lattice of Euclidean dimension $\bar{d}$ (proved for the Spherical and $O(\infty)$ models[12]) still holds for the $O(2)$ model. Were these assumptions satisfied, a comparison with Eq. (1) would yield

$$D = \bar{d}. \tag{7}$$

We will later observe, in Sec. IV, that numerical results strongly hints that both assumptions are satisfied. In the present section we, rather, provide an analysis of the spectral dimension supporting directly the above identity, Eq. 7. We numerically estimated the spectral dimension of 2D dilute Lévy graphs, with several values of the power ρ, through the calculation of the probability of self-return of a random walker in the graph after a time τ, $P(\tau)$, a quantity related[55] to the spectral dimension via

$$P(\tau) \sim \tau^{-\bar{d}/2} \tag{8}$$

for large τ. Our results are summarized in Fig. 3, in which we compare $D(\rho)$ in Eq. (1) with the estimation

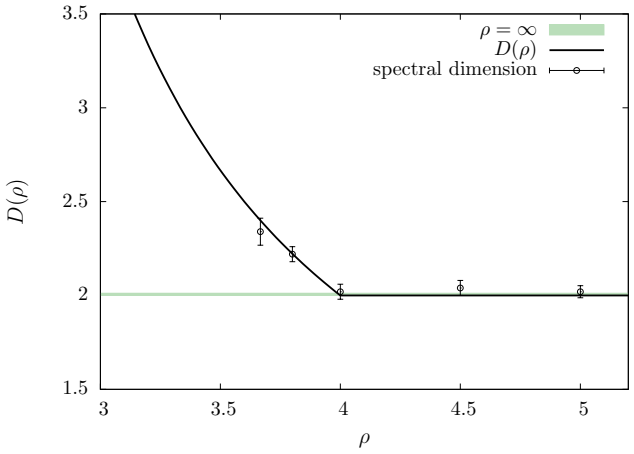

FIG. 3: Equivalent short-range dimension $D(\rho)$, Eq. (1), and numerically estimated spectral dimension $\bar{d}$ versus ρ. The light full line is the square lattice case.

of $\bar{d}$ at the corresponding ρ *via* the histogram of the random walker self-return times. Details of the method are reported in App. A.

Fig. 3 suggests the equivalence between the spectral dimension of the graph $\bar{d}$, and the short-range dimension D. This implies that the ρ-dependence of the spectral dimension of the Lévy graph with power ρ is as its equivalent fully connected version, Eq. 6, and that the $O(2)$ model criticality in a graph is exclusively determined by its spectral dimension.

III. NUMERICAL METHOD, ALGORITHM AND DETAILS OF THE SIMULATION

We now expose the numerical method used to analyze the critical properties of the XY model in dilute 2D lattices (3), via Monte Carlo sampling in finite size realizations of graphs with N vertices and $2N$ edges. Given T and ρ, we consider both the ensemble average, at T, and the graph (topology) average at ρ:

$$\langle O \rangle = \sum_{\{J\}} \sum_{\{\mathbf{S}\}} O\{\mathbf{S}\} \, \exp\left[-H\{\mathbf{S}\}/T\right] \mathcal{P}_\rho(J), \qquad (9)$$

where H is the Hamiltonian of the model (3) and O is an observable. The following quantities are measured: the specific heat

$$c = \frac{1}{N} \frac{\partial \langle H \rangle}{\partial T} = \frac{1}{NT^2} \left(\langle H^2 \rangle - \langle H \rangle^2 \right); \qquad (10)$$

the susceptibility and the fourth-order Binder cumulant:

$$\chi = N \langle |\mathbf{m}|^2 \rangle, \qquad U_4 = \frac{\langle |\mathbf{m}|^4 \rangle}{\langle |\mathbf{m}|^2 \rangle^2} - 1; \qquad (11)$$

where $\mathbf{m}$ is the observable magnetization:

$$\mathbf{m} = \frac{1}{N} \sum_{j=1}^{N} \mathbf{S}_j, \qquad (12)$$

and where $\{\mathbf{S}_j\}_{j=1}^N$ is a given configuration. Finally, and only in the square lattice case, we also measure the second moment correlation length ξ_2[56]:

$$\xi_2 = \frac{1}{2 \sin(\mathbf{k}_{\min}/2)} \left[\frac{\chi(\mathbf{0})}{\chi(\mathbf{k}_{\min})} - 1 \right]^{1/2} \qquad (13)$$

where $\mathbf{k}_{\min}$ is the smallest momenta in the Fourier space corresponding to the finite-size lattice and χ is the Fourier transform of the spatial equilibrium two-point correlation function

$$C(\mathbf{r}) = \frac{1}{N} \sum_i \langle \mathbf{S}_i \cdot \mathbf{S}_{i'} \rangle \qquad (14)$$

where i' is such that $\mathbf{r}_{i'} = \mathbf{r}_i + \mathbf{r}$ for each i.

With these observables we analyze the critical properties of the model around the critical temperature T_c using the scaling relations:

$$\begin{aligned} c(T,N) &= N^{\alpha/\bar{\nu}} \, \tilde{c}(t\, N^{1/\bar{\nu}}) \\ \chi(T,N) &= N^{\gamma/\bar{\nu}} \, \tilde{\chi}(t\, N^{1/\bar{\nu}}) \\ U_4(T,N) &= \tilde{U}_4(t\, N^{1/\bar{\nu}}) \\ \xi_2(T,N) &= \tilde{\xi}_2(t\, N^{1/\bar{\nu}}) \end{aligned} \qquad (15)$$

where $t = T - T_c$, α and γ are the standard critical exponents and $\bar{\nu}$ is the correlation volume exponent. This is suited to study scaling relations in graphs and fully connected systems,[35,57] in which the correlation length is no longer well-defined, but for which the correlation volume V diverges at the critical point as $V \sim t^{-\bar{\nu}}$. The correlation volume exponent is related to the correlation length exponent by $\bar{\nu} = D_{\rm u}\, \nu$ where $D_{\rm u}$ is the upper critical dimension of the corresponding short-range system.

According to the arguments of Sec. II, and in order to elucidate the nature of the phase transition in each regime, we have run six sets of simulations with the values in the first column of Tab. III, cf. Fig. 2. We have studied finite-size realizations of the system in Lévy graphs with $N = L^2 = 2^{2n}$ nodes, $n = 4, 5, 6, 7, 8$. Each run, for a fixed topology, consists of 2^{21} Monte Carlo Steps (MCS). We measure observables each 32 MCS. Time averages are performed on exponentially increasing windows (between 2^k and 2^{k+1}, $k = 1 \ldots, 19, 20$). Topology averages are performed over a sampling of N_g simulations with different realizations of the graph topology, with N_g decreasing for increasing N, going from $N_g = 160$ for $N = 2^8$ to $N_g = 6$ for $N = 2^{16}$. Equilibration checks have been done by comparing time averages of observables on increasing exponential time windows

and verifying the consistency of the energy and magnetization histograms and the correlation length values for the last time windows. As a further equilibration test, we have checked the coincidence specific heat measurements according to both the second and third equalities in Eq. 10, cf. Fig. 7 top-left panel.

A. Details of the algorithm

We now present a more detailed description of the algorithm used: a home-made high-performance parallel code for the Monte Carlo dynamics of spin models defined on general networks. The software is developed for GPUs architecture and it has been developed with the CUDA programming model.[58] A single-spin flip Metropolis update has been used, with non-connected spins being updated in parallel by different GPU cores.

1. *Graph coloring*

This procedure requires the *coloring* of each realization of the randomly generated graph before dynamics starts. The graph nodes are colored with the same color if they are not connected to each other. During the simulation, sites with a common color are Metropolis-updated synchronously, and subsets of the set of vertices corresponding to different colors are processed sequentially on each MCS. This is a generalization of the so called Red-Black Gauss Seidel algorithm used in the parallelization of spin operations in bipartite graphs, as hyper-cubic lattices.

We approximately color the graph using a variant of the Smallest-Last-Ordering (SLO) algorithm,[59,60] costing $O[N]$. For the simulated sizes ($N \leq 2^{16}$) the number of colors (equal to two in the $\rho = \infty$ case) turns out to be never larger than 6 the worst case ($\rho = 0$). As one can see in Fig. 4, with our coloring procedure the distribution of non-interacting sets becomes more and more homogeneous as N increases, thus automatically enhancing the algorithm efficiency.[60]

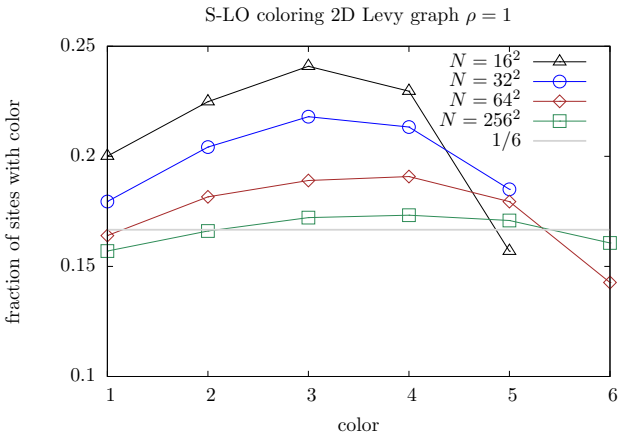

FIG. 4: Coloring a dilute Lévy 2D graph with power $\rho = 1$ and $N = L^2 = 2^{8-14}$ nodes with the SLO algorithm. The larger the graph, the more homogeneous is the partition of the set of graph nodes in subsets corresponding to different colors.

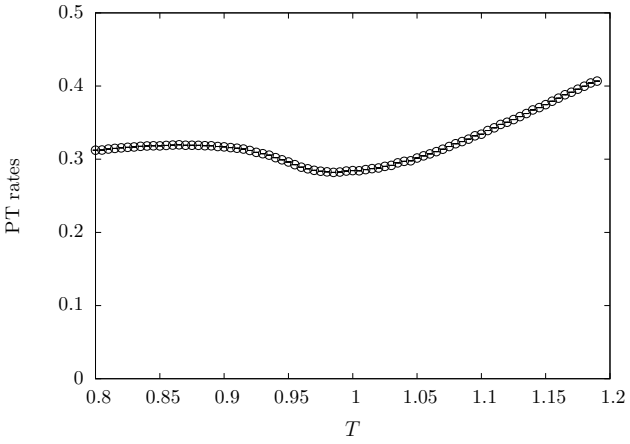

FIG. 5: Exchange rate between nearby heat baths in the PT algorithm in a square lattice with $N = 2^{16}$ sites. The distance between consecutive temperatures is $\Delta T = 0.005$.

2. *Improved equilibrium dynamics*

In our code, besides the Metropolis algorithm, also the Parallel Tempering (PT)[61] and Over-relaxation (OR)[62] algorithms are implemented. Both algorithms reduce the correlation time of the Monte-Carlo Markov processes and improve the equilibration.[77]

PT swap attempts are performed (in CPU) every MCS, with replicas at different temperatures being updated in parallel, as explained in Ref. 63. Fig. 5 illustrates the rate of PT swaps between configurations with adjacent temperatures at fixed intervals of $\Delta T = 0.005$, as a function of the temperature for a system with $N = 2^{16}$ in the 2D square lattice, for which the critical temperature is known to be $Tc = 0.8929...$.

3. *Memory management*

We have used a storage of the degrees of freedom in the *global device memory* of the GPU architecture,[63,64] each *thread* accessing the $O(2)$ angle of its corresponding graph node in such a way that sites with a common color are consecutive in the array, favoring *coalesced* memory access. Each *thread*, then, accesses an array in global memory, from which it reads the list of sites connected to the corresponding site. An independent random number generator of the Fibonacci type[63] is associated to each *device thread*, so that the random numbers are stored in *shared memory*, the values of the random number generator parameters being fixed to $r_{\rm F} = 250$, $s_{\rm F} = 128$,

with which we obtained a satisfactory quality of random numbers, as we concluded from the results of our benchmark comparison with the known results for the critical temperature of the XY model in the square lattice (see the subsection IV A). We used double floating-point precision for storing observables, and single precision for the calculation of the trigonometric functions in the evaluation of the energy and magnetization of each site. In the latter case we adopted the special fast_math function of the GPU architecture, a faster routine specific of the GPU architecture.[65]

4. *Computational speed*

We now present some details about the performance of our algorithm, referring to a calculation performed in an nVidia GPU GTX480 Fermi card. In Tab. II the reader may find the computation time per spin involved in the Metropolis and OR algorithms in a square lattice with $N = 2^{14}$ sites and PBC, for different choices of the floating point precision and of the routine used for the computation of trigonometric operations. In Fig. 6 a comparison of the computation time for the PBC square and Lévy lattice with $\rho = 7/3$ with different sizes is shown. Since in a general graph colored with Q colors our algorithm is nearly $Q/2$ times slower than the code in the square lattice, we also show $2/Q$ times the computation time in the Lévy graph for comparison with the square lattice case. The minimum time peaks for Metropolis and OR algorithms are 0.55ns and 0.36ns respectively, a mark which is competitive with state-of-the-art highly-optimized GPU simulations of spin glasses,[66] (a direct comparison is not possible since their benchmark refers to the $O(3)$ model) and represents a speedup of more that five hundred times with respect to a serial C-code running on an Intel i7 CPU with 2.67GHz. In the next section some accuracy benchmarks of the code are presented. All of the simulations in this work have been performed using single precision (4 bytes) for the storing of floating-point numbers and the fast_math CUDA functions. We ran simulations changing both precision and trigonometric routines, and introducing OR sweeps, without finding essential accuracy improvements. An upgraded and generalized version of this algorithm, designed for the study of random laser modes[67–70] in arbitrary topologies, will be extensively reviewed and presented in a forthcoming work.[60]

IV. NUMERICAL RESULTS

In this section we present numerical results supporting the considerations about the XY model criticality as a function of ρ that we presented in section II. All shown results are obtained with PBC, since no large quantitative difference is found adopting FBC (see Sec. II).

algorithm	precision	trig. function	time per spin [ns]
MET + PT	single	fast	1.88
MET	single	fast	0.635
MET	single	cosf	0.865
OR	single	fast	0.36
OR	single	cosf	0.54

TABLE II: Computational time of different algorithms per spin. It is the total computation time of a run divided by N, by the number of copies N_T at different temperatures in the PT algorithm and by the number of MCS's.

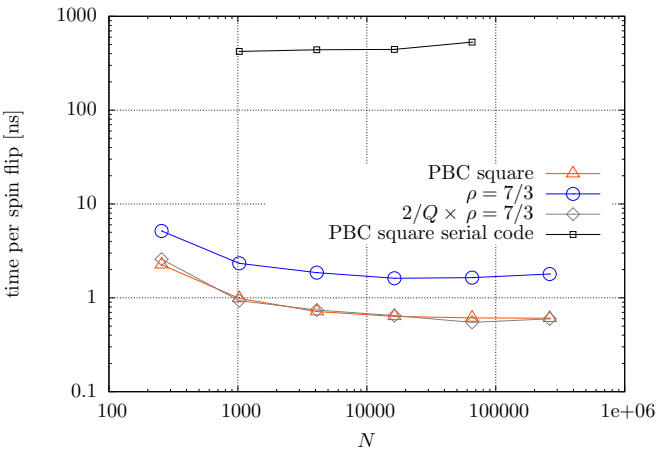

FIG. 6: Computational time per spin of the Metropolis algorithm versus N for the square nearest-neighbor lattice and $\rho = 7/3$ Lévy lattice. The serial-CPU run is shown for comparison: a speedup of several hundreds of times can be observed.

A. Kosterlitz-Thouless transition: 2D square lattice limit

As a benchmark test we have analyzed the outcome of our algorithm in the square lattice (the $\rho = \infty$ limit), where the XY model is known to undergo an infinitely high order transition, the KT transition.[16,17] The paramagnetic high temperature phase, in which vortices *unbound*, displays exponentially decaying spatial correlations. The low temperature spin-wave phase is made of coupled pairs of vortices of opposite chirality. It is characterized by the absence of spontaneous magnetization and a power-law asymptotic decay of the spatial correlation function. Critical exponents depend on the temperature.

We can compare our results with the analysis of Ref. 71, finding excellent agreement for all the analyzed quantities (χ, $\langle H \rangle$, ξ_2, c). As a further test, we have looked at several properties of the KT transition, that we will also consider as fingerprints for the classification that we will do in the following, cf. Sec. IV E. We enumerate them for clarity:

1. *Absence of magnetization.* In particular, we find numerical evidence of vanishing $\langle|\mathbf{m}|\rangle$.[78] At temperature larger than the critical point one observes a clear behavior $\langle|\mathbf{m}|\rangle(T,N) \sim N^{-1/2}$. At lower temperatures, though the decrease with N is slower, it is still a decreasing function of N, a behavior compatible with $\langle|\mathbf{m}|\rangle = 0$ in the thermodynamic limit. As we will see in the following this behavior is typical for the whole short-range regime, cf. Fig. 12. The slow decrease is compatible with logarithmic corrections of the type $X(N) \sim (c+\ln N)^{-1} + O[(c+\ln N)^{-2}]$, characteristic of the KT transition.[72]

2. *Exponential divergence: Kosterlitz-Thouless law.* Susceptibility and correlation length behave at criticality as[17]

$$X = X_0 \exp\left\{\frac{b_X}{\sqrt{t}}\right\} \tag{16}$$

with $t = T - T_c > 0$ and $X = \xi_2, \chi$. Figure 8, top left panel, illustrates this behavior interpolating the largest simulated size. Remarkably, our estimation of T_c from the fit with the KT law for χ gives $T_c = 0.892(9)$, in excellent agreement with state-of-the-art accurate estimations[72] of T_c, =0.8929(4), and the estimate from the KT law for ξ_2 is $T_c = 0.90(2)$.

3. *Continuous specific heat at the transition*, as illustrated in Fig. 7, top left panel.

4. *Scale invariance in the whole range $T \leq T_c$.* The scaling functions ξ_2/L and U_4 are scale invariant for all $T < T_c$ in the large-N limit.[73] Differently from what happens, for example, in a second-order phase transition, one observes a superposition of the finite-size ξ_2/L curves corresponding to different, sufficiently large, values of L (see inset of Fig. 8, top left panel).

B. Erdös-Rényi limit

For completeness and checking we have also studied the $\rho = 0$ limit, corresponding to a random, or Erdös-Rényi graph with a Poisson distribution of the degree of connectivity and average degree equal to 4. We report numerical evidence for a second-order mean-field phase transition. Our results are compatible with the theoretical values of the critical exponents $\bar{\nu} = 2$, $\gamma = 1$ and $\alpha = 0$, as argued in section II, and are in agreement with the numerical estimates of Refs. 35,36, where the mean-field transition on Erdös-Rényi graphs of average degree 3 and 8, respectively, have been analyzed.

As in the previous subsection, we now present the salient analysis for the Erdös-Rényi case. The critical temperature can be estimated from the scaling of the value at which the finite-size cumulant $U_4(T,N)$ intersects with $U_4(T,N/4)$, a value that we call $T(N)$. Assuming the finite-size scaling $T(N) = CN^{-1/\bar{\nu}} + T_c$, we obtain $T_c = 1.93(4)$, in agreement with the analytic value $T_c = 1.9361$.[74] The exponent $\bar{\nu}$ may be calculated from the relation

$$\left.\frac{\partial U_4(T,N)}{\partial T}\right|_{U_4=\text{const}} \propto N^{1/\bar{\nu}} \tag{17}$$

where the derivative of U_4 with respect to the temperature is evaluated at fixed values of U_4 in the scaling critical region. Approximating the derivative with a finite difference (and using the standard deviation of $\dot{U}_4$ as an input error for the fit) we obtain $\bar{\nu} = 2.00(2)$, in agreement with the mean-field value $\bar{\nu} = 2$. Further numerical evidence for the mean-field values may be found in the scaling of the functions U_4, χ and c (see Figs., e.g, 9, 8, 7). We remark that, although the value of the critical exponents is the mean field one, the value of the critical temperature is not a universal quantity and does not coincide with the Gaussian mean-field value[13] $T = 2$. We also checked the relation $2\beta+\gamma = 2-\alpha$ by observing the right scaling of the magnetization with the mean-field exponent $\beta = 1/2$. Indeed, an important feature of this mean-field transition is that the low-temperature phase presents a finite magnetization, and this is confirmed by finite size scaling analysis of $\langle|\mathbf{m}|\rangle$ in the low T phase (the numerical behaviors are analog to other mean-field cases, see, e.g., Fig. 10).

C. Long-range mean-field regime

We repeated the same analysis for $\rho = 14/6$ and $17/6$, in the mean-field regime. The first value is nearer to the limit of convergence, $\rho = d = 2$, of the fully connected model, where the largest differences with the dilute model could possibly arise. The second value of ρ is very near the mean-field threshold $\rho_{\rm mf} = 3d/2 = 3$. Through finite size scaling of the Binder cumulant we estimate $T_c = 1.94(1)$ and $T_c = 2.00(1)$, respectively. The derivative of U_4 with respect to T allows to estimate $\bar{\nu} = 2.01(1)$ and $\bar{\nu} = 1.99(3)$. These are both compatible with mean-field theory.

Indeed, the system in the mean-field regime behaves as a short-range system in $D_{\rm u} = 4$ dimensions, hence displaying the correlation length exponent $\nu = 1/2$. The correlation volume in the short-range system is the $D_{\rm u}$-th power of the correlation length, and diverges as

$$\xi^{D_{\rm u}} \sim t^{-D_{\rm u}/\nu_{\rm mf}}$$

when $t \to 0$. Since both systems have common critical exponents,[57] the above scaling implies, cf. Sec. III.

$$\bar{\nu} = \frac{D_{\rm u}}{\nu} = 2 \tag{18}$$

Let us now consider the correlation length exponent in the short-range equivalent system in $D(\rho)$-dimensions,

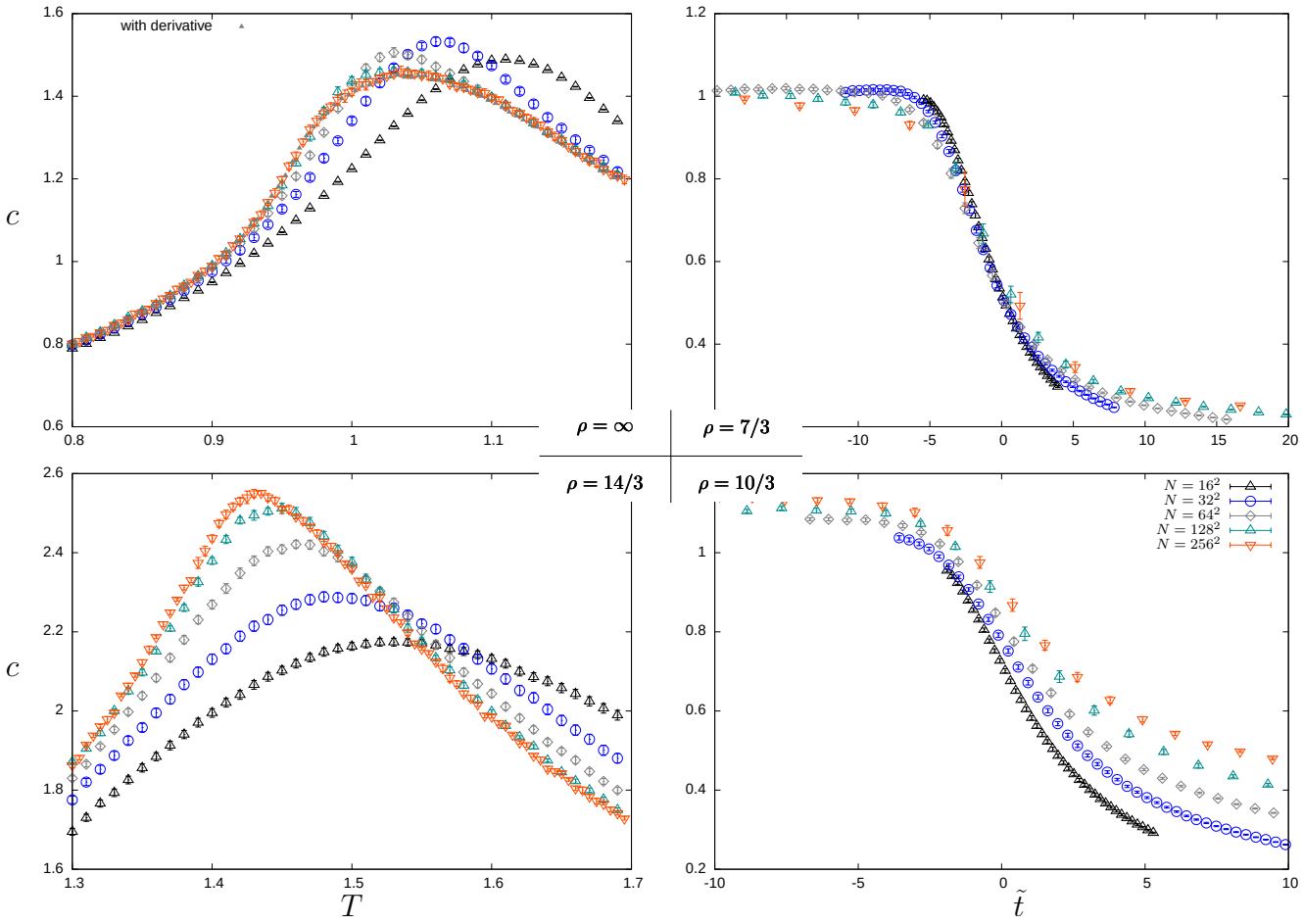

FIG. 7: Specific heat versus temperature and $\tilde{t} = t\,N^{1/\bar{\nu}}$ for different Lévy lattices and sizes $N = 2^{2n}$, $n = 4, \ldots, 8$. Top-left: 2D PBC XY model. Top-right: dilute model with $\rho = 7/3$ in the mean-field regime, $\nu = 2.01(1)$. Bottom-right: dilute model with $\rho = 10/3$ in the long-range non-mean-field regime, $\nu = 2.21(1)$. Bottom-left: dilute model with $\rho = 14/3$ in the short-range regime. The large N limit of this function is regular and continuous (see the main text).

that we called ν_ρ in section I. It may be inferred, as in reference 43, comparing the scaling of the free energy density of the original system in d dimensions, proportional to $\xi^{-d} \sim t^{-d/\nu}$, and the free energy density of the equivalent short-range D-dimensional system, $\xi^{-D} \sim t^{-D/\nu_\rho}$. It follows:

$$\nu_\rho = \nu\,\frac{D(\rho)}{d} = \frac{1}{\rho - d}, \tag{19}$$

which coincides with ν_ρ found in Ref. 44, as mentioned in Sec. I.

In Fig. 7, top-right panel, one observes a scaling of the type $c(T, N) = \tilde{c}(t\,N^{1/2})$, suggesting that $\alpha = 0$. We estimated the γ exponent by fitting it from the numerical estimates for the function $\ln \chi(T, N) = \gamma/\nu \ln N + \ln \tilde{\chi}(\tilde{t})$ as a function of $\ln N$ for a fixed value of $\tilde{t} = t\,N^{1/\bar{\nu}}$ in the scaling regime, obtaining $\gamma = 0.98(4)$ (c.f. figure 8, top-right panel). Finally, one finds (see Fig. 10) that there is spontaneous magnetization in the low-temperature phase.

These numerical results strongly support that the system belongs to the mean-field universality class in the range $\rho \in [0 : 3d/2]$. In the whole range the critical exponents $\bar{\nu} = 2$, $\gamma = 1$, $\alpha = 0$ are well defined. On the other hand, the correlation length exponent of the equivalent short-range system, ν_ρ in Eq. 19, is no longer defined for $\rho \leq d$, where the dimensionality D diverges.

D. Long-range non-mean-field regime

An analogous analysis leads to a different behavior in the non-mean-field regime, for $\rho = 10/3$. For the critical temperature we estimate $T_c = 1.749(6)$. The finite-size scaling analysis of Eq. (17) reveals a correlation volume exponent larger that the mean-field value 2: $\bar{\nu} = 2.21(1)$ (see Fig. 11). Estimating the γ exponent from the N

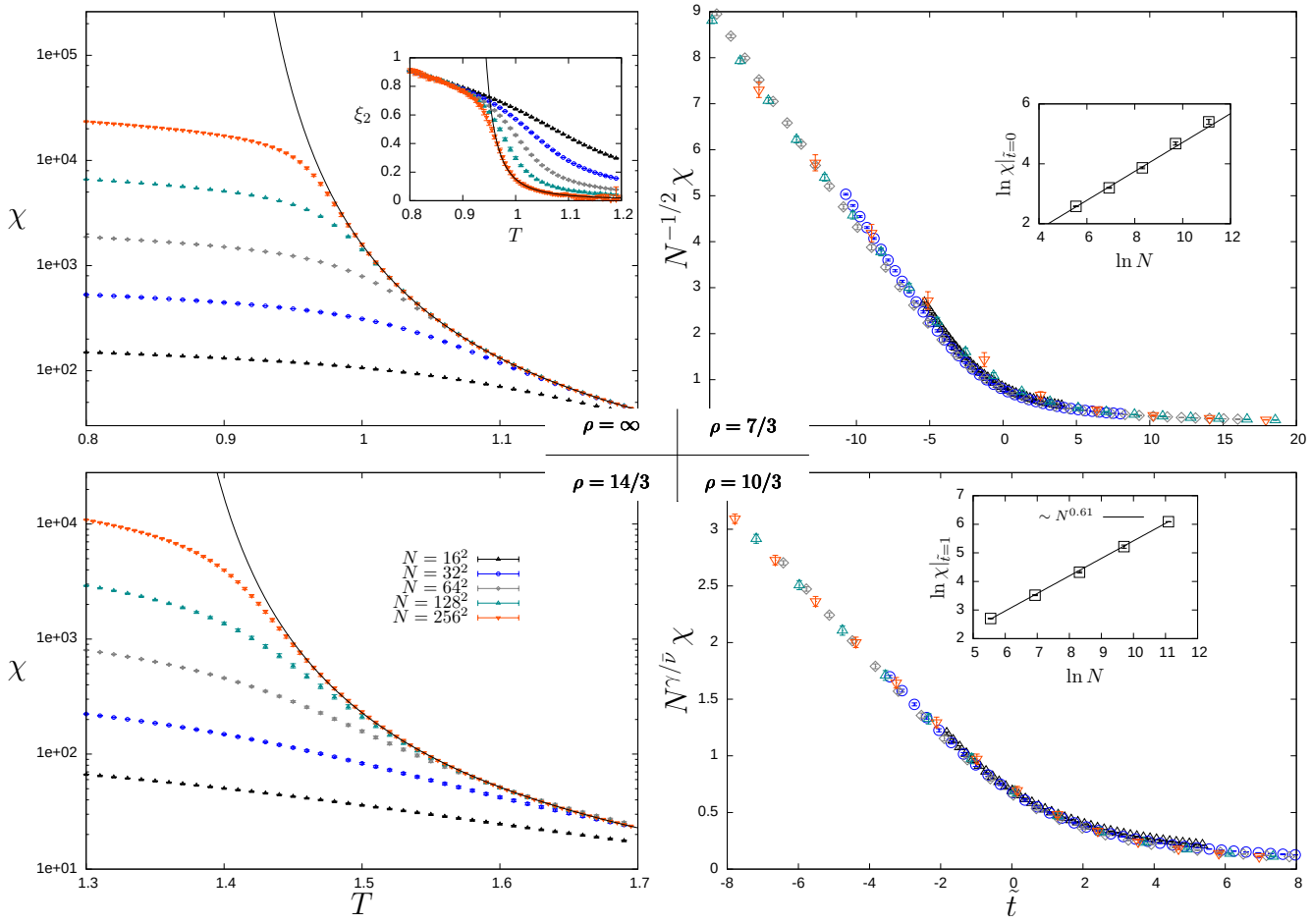

FIG. 8: Magnetic susceptibility versus temperature for different Lévy graphs (ρ and L values are as in Fig. 7). Top-left: 2D PBC XY model. As the size increases, $\chi(T)$ becomes more and more similar to the functional law Eq. (16). For $N = 2^{16}$ it is $\ln \chi_0 = -1.48(2)$, $b_\chi = 2.89(1)$ and $T_c = 0.8929(4)$. Inset: correlation length. Also in this case the large size limit obeys Eq. (16), with $\ln \xi_0 = -6.5(7)$ and $b_\xi = 1.4(4)$. In the low-temperature phase the ξ_2 curves collapse. Top-right: Scaling of the susceptibility for the mean-field Lévy model at $\rho = 7/3$, cf . Eq. (15). Inset: finite size behavior of $\ln \chi$ at fixed $\tilde{t}$, leading to $\gamma = 0.98(4)$. Bottom-right: Scaling of the susceptibility for the long-range non-mean-field model at $\rho = 10/3$ for $T > T_c$. The critical exponents are $\bar{\nu} = 2.21(1)$, $\gamma = 1.34(2)$. Bottom-left: susceptibility vs. temperature for the Lévy short-range case, $\rho = 14/3$. The KT fit gives $\ln \chi_0 = -1.52(2)$, $b_\chi = 2.80(2)$ and $T_c = 1.338(1)$.

dependence of the function $\ln \chi(T, N)$ for a fixed value of the scaling variable $\tilde{t}$, we obtain $\gamma = 1.34(1)$, c.f., Fig. 8 bottom-right panel, different from the mean-field value, 1. On the other hand, the specific heat data is compatible with $\alpha = 0$. Indeed, although the N-dependence of the specific heat is slower with respect to the mean-field case, the data in Fig. 7, bottom-right panel, suggest that curves corresponding to different N's collapse in the large-N limit for common values of $\tilde{t}$. Finally, we observe a low-T magnetized state, $\langle |\mathbf{m}| \rangle \neq 0$.

E. Short-range Regime

The case $\rho = 14/3$ in the short-range regime presents all the features that we presented as numerical fingerprints of the KT transition in subsection IV A: *(1)* the low-T phase is unmagnetized, as deduced from the decreasing behavior of $\langle |\mathbf{m}| \rangle$ vs. N for the sizes studied, cf. Fig. 12; *(2)* The KT law, Eq. (16) is satisfied, yielding an estimate $T_c = 1.338(1)$, cf. Fig. 8, bottom-left panel; *(3)* the specific heat is not divergent nor discontinuous at the transition, cf., Fig. 7, bottom-left panel, at difference with the other cases, in which the discontinuity of c was reflected in the discontinuity of the derivative of its scaling function, $\tilde{c}$; *(4)* A numerical evidence of the fact that the quantity U_4 is scale invariant for sufficiently large sizes is shown in Fig. 13, in which one observes that the quantity $|U_4(T, N) - U_4(T, 4N)|$ decreases for increasing values of N at constant values of T immediately below the transition.

We summarize all our results in Tab. III.

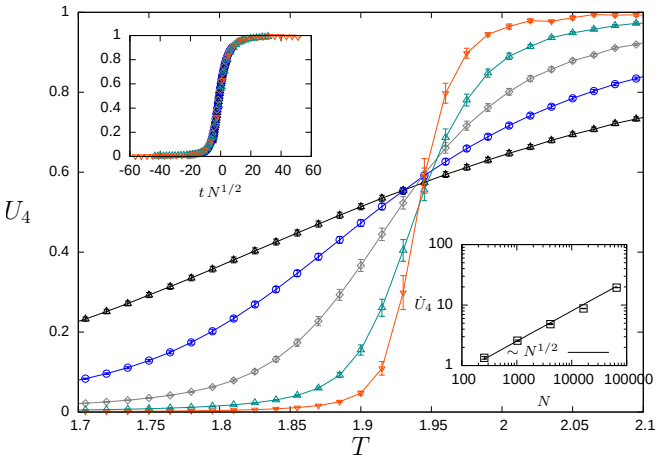

FIG. 9: Binder cumulant versus temperature for $\rho = 7/3$ in the mean-field regime. The upper inset shows the scaling (15) with $\bar{\nu} = 2.07(9)$ and the lower inset is the calculation of $\bar{\nu}$ with the relation (17).

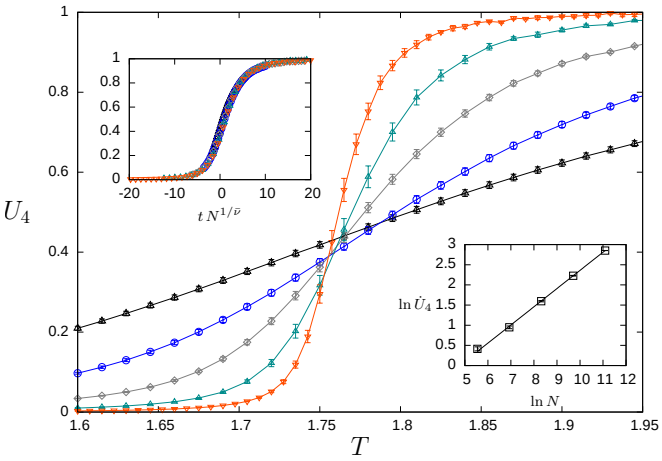

FIG. 11: Binder cumulant versus temperature for $\rho = 10/3$ in the non-mean-field regime. The insets are as in figure 9 with $\bar{\nu} = 2.21(1)$.

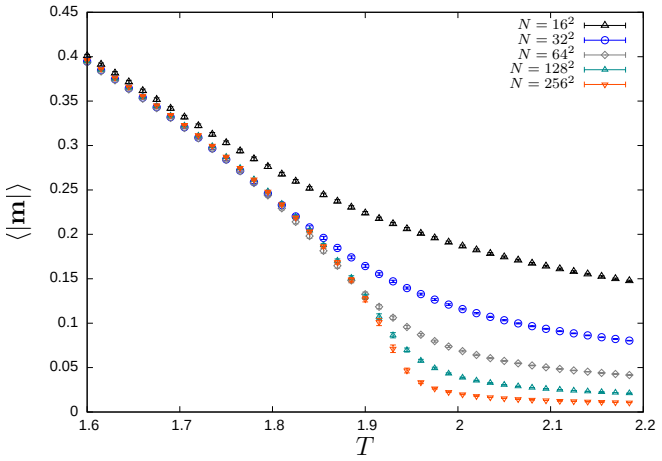

FIG. 10: Magnetization versus temperature for $\rho = 7/3$ in the mean-field regime. The low temperature phase exhibits spontaneous magnetization.

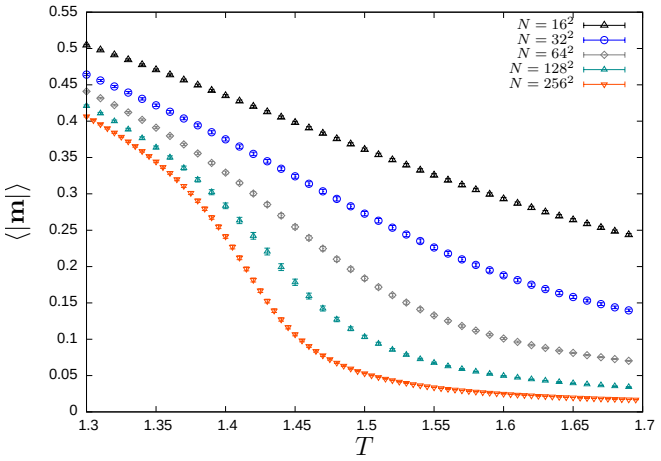

FIG. 12: Magnetization versus temperature for $\rho = 14/3$ in the short-range regime. In the low-T phase the magnetization monotonously decreases with N, indicating that this phase does not exhibit spontaneous magnetization.

V. CONCLUSIONS AND PERSPECTIVES

Extensive numerical simulations on the 2D Lévy lattice yield evidence for three different critical regimes, corresponding to given intervals in the Lévy exponent ρ governing the topology of the graphs: short-range $\rho \in [2+d, \infty)$, non-mean-field long-range $\rho \in (3d/2, 2+d)$ and mean-field $\rho \in [0, 3d/2]$. For each value of ρ, the critical behavior is in a one-to-one correspondence with that of a short-range XY model in D dimensions. This short-range effective dimension is $D = d$ for $\rho \geq 2 + d$, while it is $D = 2d/(\rho - d)$ for $\rho \in (d, 2+d)$, in the long-range and part of the mean-field regime. As $\rho \to d$, it tends to infinite. This is the value of ρ for which the fully connected version of the model displays a divergent energy.

In the mean-field regime we measured the standard mean-field exponents $\gamma = 1$, $\alpha = 0$ and $\bar{\nu} = 2$. The latter is the correlation volume exponent, related with the correlation length exponent $\nu = \bar{\nu}/D_{\mathrm{u}} = 1/2$. These exponents agree with the already mentioned theoretical predictions for the D-dimensional equivalent model in the mean-field regime: ν_ρ, η_ρ, γ_ρ (see subsection IV C). In the non-mean field regime, instead, we find a continuous phase transition with different critical exponents and a low-temperature phase exhibiting spontaneous symmetry breaking. Finally, we report evidences for the onset of a KT-like transition in the short-range regime.

The hypothesis presented in Sec. II, that D is the

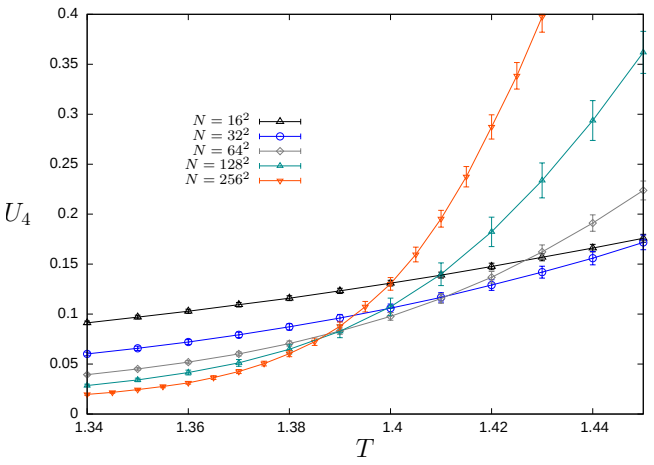

FIG. 13: Binder cumulant versus temperature for $\rho = 14/3$ in the short-range regime. There is evidence for the scale-invariance of this quantity for $T < T_c$ in the large-N limit.

ρ	0	14/6	17/6	20/6	28/6	∞
T_c	1.932(1)	1.94(1)	2.00(1)	1.749(6)	1.338(1)	0.892(9)
$\bar{\nu}$	2.00(2)	2.01(1)	1.99(3)	2.21(1)	-	-
γ	1.00(1)	0.98(4)	1.04(8)	1.34(2)	-	-
α	0	0	0	< 0.1	-	-
$\langle \lvert\mathbf{m}\rvert \rangle$	$\neq 0$	$\neq 0$	$\neq 0$	$\neq 0$	$= 0$	$= 0$
UC	MF	MF	MF	NMF	SR	SR

TABLE III: Numerical results for the critical exponents and the critical properties of the XY model in different Lévy graphs. $\rho = \infty$ stays for the 2D square lattice with PBC. UC stays for "universality class": MF=mean field, NMF=non-mean-field, SR=short-range.

spectral dimension of the dilute graph, appears to be confirmed in the three regimes. The numerical data presented in section IV suggest that the low-temperature phase of the XY Lévy model in the short-range regime is not magnetized, while there is a spontaneous symmetry breaking for $\rho < \rho_{\rm sr} = 2 + d$. The already mentioned generalized Mermin-Wagner theorem for the XY model in graphs[14,15] would, then, imply that $\bar{d} = 2$ for $\rho > 4$, while $\bar{d} > 2$ for $\rho < 4$ in the dilute lattice, in agreement with Eq. (6). On the other hand, for $\rho \lesssim 4$, the identification $D = \bar{d}$ appears to be confirmed by a numerical estimation, see figure 3 and App. A. Furthermore, for $\rho \to d$, D diverges. An infinite spectral dimension, indeed, occurs in the Bethe lattice limit and, generally, in any graphs not satisfying the polynomial growth condition.[55]

The result $D = \bar{d}$ would imply that the critical behavior of the $O(2)$ model on a graph characterized by a spectral dimension $\bar{d}$ coincides with the one of the short-range $\bar{d}$-dimensional $O(2)$ model, allowing for a deeper understanding of the physics of interacting systems on non-regular structures and extending the known universal properties of the spectral dimension of the $O(n \to \infty)$ model[11] to finite n.

Summarizing, we have found that the critical properties of the $O(2)$ model in a graph can be divided in three regimes characterized by the spectral dimension of the graph, which plays the role of the dimension of a short-range model with common critical properties. As a perspective, we propose to investigate how the introduction of disorder changes this scenario.[54] This is the object of an ongoing research.

VI. ACKNOWLEDGMENTS

We acknowledge Raffaella Burioni for very interesting discussions. We thank the QUonG initiative of the INFN APE group for the use of their GPU cluster. The research leading to these results has received funding from the People Programme (Marie Curie Actions) of the European Union's Seventh Framework Programme FP7/2007-2013/ under REA grant agreement n 290038, NETADIS project and from the Italian MIUR under the Basic Research Investigation Fund (FIRB/2008) program grant No. RBFR08M3P4.

Appendix A: Spectral density estimation

In order to estimate $\bar{d}$ we have studied the histogram of return times of a collectivity of 4.10^4 random walkers averaging over 20 different finite size realizations of 2D dilute graphs with sizes $N = 128^2$ and 196^2 and 6 different values of the the power $\rho = \infty$, 5, 4.5, 4, 3.8 and 11/3. Such a histogram is proportional to the probability of self-return of a random walker in the graph after a time τ: $P(\tau)$. For large values of $\rho > 2 + d$ and in the square lattice case the estimation of $\bar{d}$ is very accurate since the function P presents a very clear power-law behavior even at large times and finite-size effects are not an issue. For smaller values of ρ, however, such a measure becomes less and less accurate. This is due to the presence of "shortcuts" on the graph that take the walker to the boundaries of the original lattice, where the probability P is overestimated, and to the existence of low-connected nodes. To cope with these drawbacks, for $\rho > 4$ our random walkers start from the center of the original finite-size 2D lattice, while for $\rho \leq 4$, each realization of the walker starts from a node which is chosen at random between the subset of nodes whose degree is larger than two. In Fig. 14 we present the P histograms (up to an arbitrary, ρ-dependent constant) for each studied value of ρ, from which the data of Fig. 3 have been inferred.

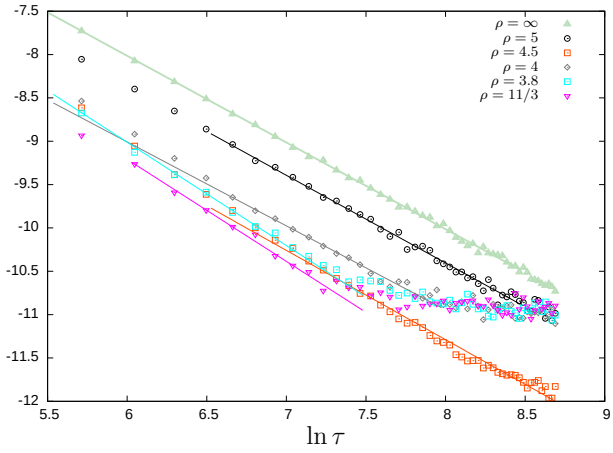

FIG. 14: Logarithm of the histogram of self-return times of a random walker in dilute 2D graphs of size $N = 196^2$ with different values of ρ. Points are the numerical measures, while lines are the fits with a linear function (their endpoints indicate the corresponding fit intervals). The slope of the fits is -2 times the spectral dimension (see figure 3).

* Electronic address: miguel.berganza@roma1.infn.it; Electronic address: luca.leuzzi@cnr.it

[1] A. Krawiecki, J. A. Hołyst, and D. Helbing, Phys. Rev. Lett. **89**, 158701 (2002).
[2] J.-S. Yang, S. Chae, W.-S. Jung, and H.-T. Moon, Physica A **363**, 377 (2006).
[3] J.-S. Yang, W. Kwak, T. Kaizoji, and I.-m. Kim, Eur. Phys. J. B **61**, 241 (2008).
[4] J. S. Yang, W. Kwak, G. Kwang-Il, and I. Kim, Europhys. Lett. **84**, 36004+ (2008).
[5] W. Bialek, A. Cavagna, I. Giardina, T. Mora, E. Silvestri, M. Viale, and A. M. Walczak, PNAS **109**, 4786 (2012).
[6] L. de Arcangelis and H. J. Herrmann, PNAS **107**, 3977 (2010).
[7] D. De Martino, M. Figliuzzi, A. De Martino, and M. E., PLoS Comput. Biol. **8**, e1002562 (2012).
[8] A. De Martino, D. De Martino, R. Mult, and G. Uguzzoni, PLoS ONE **7**, e39849 (2012).
[9] S. N. Dorogovtsev, A. V. Goltsev, and J. F. F. Mendes, Rev. Mod. Phys. **80**, 1275 (2008), arXiv:0705.0010 .
[10] H. E. Stanley, Phys. Rev. Online Archive (Prola) **176**, 718 (1968).
[11] R. Burioni, D. Cassi, and C. Destri, Phys. Rev. Lett. **85**, 1496 (2000).
[12] D. Cassi and L. Fabbian, J. Phys. A **32**, L93+ (1999).
[13] K. Hattori, T. Hattori, and H. Watanabe, Prog. Theor. Phys. Supp. **92**, 108+ (1987).
[14] R. Burioni, D. Cassi, and A. Vezzani, Phys. Rev. E **60**, 1500 (1999).
[15] D. Cassi, Phys. Rev. Lett. **68**, 3631 (1992).
[16] J. M. Kosterlitz and D. J. Thouless, J. Phys. C **6**, 1181 (1973).
[17] J. M. Kosterlitz, J. Phys. C **7**, 1046 (1974).
[18] N. D. Mermin and H. Wagner, Phys. Rev. Lett. **17**, 1133 (1966).
[19] A. Barrat and M. Weigt, Eur. Phys. J. B **13**, 547 (2000).
[20] M. Gitterman, J. Phys. A **33**, 8373 (2000).
[21] C. P. Herrero, Phys. Rev. E **65**, 066110 (2002).
[22] H. Hong, B. J. Kim, and M. Y. Choi, Phys. Rev. E **66**, 018101 (2002).
[23] W. Kwak, J. S. Yang, J. I. Sohn, and I. M. Kim, Phys. Rev. E **75**, 061130+ (2007).
[24] G. Bianconi, Phys. Lett. A **303**, 166 (2002).
[25] A. Aleksiejuk, J. A. Hoyst, and D. Stauffer, Physica A **310**, 260 (2002).
[26] M. Leone, A. Vazquez, A. Vespignani, and R. Zecchina, Eur. Phys. J. B **28**, 191+ (2002).
[27] S. N. Dorogovtsev, A. V. Goltsev, and J. F. F. Mendes, Phys. Rev. E **66**, 016104+ (2002).
[28] C. P. Herrero, Phys. Rev. E **69**, 067109+ (2004).
[29] M. Bauer, S. Coulomb, and S. N. Dorogovtsev, Phys. Rev. Lett. **94**, 200602+ (2005).
[30] D. S. Callaway, J. E. Hopcroft, J. M. Kleinberg, M. E. J. Newman, and S. H. Strogatz, Phys. Rev. E **64**, 041902+ (2001).
[31] S. N. Dorogovtsev, Phys. Rev. E **67**, 045102+ (2003).
[32] F. Iglói and L. Turban, Phys. Rev. E **66**, 036140+ (2002).
[33] S. N. Dorogovtsev, A. V. Goltsev, and J. F. F. Mendes, Eur. Phys. J. B **38**, 177 (2004).
[34] E. Khajeh, S. N. Dorogovtsev, and J. F. F. Mendes, Phys. Rev. E **75**, 041112+ (2007).
[35] B. J. Kim, H. Hong, P. Holme, G. S. Jeon, P. Minnhagen, and M. Y. Choi, Phys. Rev. E **64**, 056135+ (2001).
[36] J.-S. Yang, K.-I. Goh, I.-m. Kim, and W. Kwak, New J. Phys. **11**, 063048+ (2009).
[37] L. Leuzzi, G. Parisi, F. Ricci-Tersenghi, and J. J. Ruiz-Lorenzo, Phys. Rev. Lett. **101**, 107203+ (2008).
[38] A. Enter and J. Hemmen, J. Stat. Phys. **32**, 141 (1983).

[39] G. Kotliar, P. W. Anderson, and D. L. Stein, Phys. Rev. B **27**, 602 (1983).
[40] R. Bhatt and A. Young, J. Mag. Mag. Mat. **5457, Part 1**, 191 (1986).
[41] M. Campanino, E. Olivieri, and A. Enter, Comm. Math. Phys. **108**, 241 (1987).
[42] L. Leuzzi, J. Phys. A **32**, 1417+ (1999).
[43] D. Larson, H. G. Katzgraber, M. A. Moore, and A. P. Young, Phys. Rev. B **81**, 064415+ (2010).
[44] M. E. Fisher, S. K. Ma, and B. G. Nickel, Phys. Rev. Lett. **29**, 917 (1972).
[45] M. Picco, arXiv:1207.1018 (2012).
[46] R. A. Baños, L. A. Fernández, V. Martín-Mayor, and A. P. Young, Phys. Rev. B **86**, 134416 (2012).
[47] L. Leuzzi, G. Parisi, F. Ricci-Tersenghi, and J. J. Ruiz-Lorenzo, Phil. Mag. **91**, 1917 (2011).
[48] L. Leuzzi, G. Parisi, F. Ricci-Tersenghi, and J. J. Ruiz-Lorenzo, Phys. Rev. Lett. **103**, 267201 (2009).
[49] H. G. Katzgraber, D. Larson, and A. P. Young, Phys. Rev. Lett. **102**, 177205+ (2009).
[50] A. Sharma and A. P. Young, Phys. Rev. B **84**, 014428 (2011).
[51] D. X. Viet and H. Kawamura, Phys. Rev. Lett. **105**, 097206 (2010).
[52] A. Sharma and A. P. Young, Phys. Rev. B **83**, 214405 (2011).
[53] F. Beyer, M. Weigel, and M. A. Moore, Phys. Rev. B **86**, 014431+ (2012).
[54] R. Burioni and D. Cassi, Mod. Phys. Lett. B **11**, 1095+ (1997).
[55] R. Burioni and D. Cassi, J. Phys. A **38**, R45+ (2005).
[56] D. J. Amit and V. Martín-Mayor, *Field Theory, The Renormalization Group, And Critical Phenomena*, edited by W. Scientific (2005).
[57] R. Botet, R. Jullien, and P. Pfeuty, Phys. Rev. Lett. **49**, 478 (1982).
[58] "https://developer.nvidia.com/," ().
[59] D. W. Matula and L. L. Beck, J. ACM **30**, 417 (1983).
[60] M. I. Berganza and L. Leuzzi, In preparation.
[61] K. Hukushima and K. Nemoto, J. Phys. Soc. Jpn. **65**, 1604 (1996).
[62] M. Creutz, Phys. Rev. D **36**, 515 (1987).
[63] M. Weigel, J. Comp. Phys. **231**, 3064 (2012).
[64] E. E. Ferrero, J. P. De Francesco, N. Wolovick, and S. A. Cannas, Comp. Phys. Comm. **183**, 1578 (2012).
[65] "https://developer.nvidia.com/get-started-cuda-cc," ().
[66] T. Yavors'kii and M. Weigel, Eur. Phys. J. - Special Topics **210**, 159 (2012).
[67] H. Cao, Waves Random Media **13**, R1 (2003).
[68] D. S. Wiersma, Nature Phys. **4**, 359 (2008).
[69] L. Leuzzi, C. Conti, V. Folli, L. Angelani, and G. Ruocco, Phys. Rev. Lett. **102**, 083901 (2009).
[70] C. Conti and L. Leuzzi, Phys. Rev. B **83**, 134204+ (2011).
[71] R. Gupta, J. DeLapp, G. G. Batrouni, G. C. Fox, C. F. Baillie, and J. Apostolakis, Phys. Rev. Lett. **61**, 1996 (1988).
[72] M. Hasenbusch, J. Phys. A **38**, 5869 (2005).
[73] H. G. Ballesteros, A. Cruz, L. A. Fernández, V. Martín-Mayor, J. Pech, J. J. Ruiz-Lorenzo, A. Tarancón, P. Téllez, C. L. Ullod, and C. Ungil, Phys. Rev. B **62**, 14237 (2000).
[74] F. Morone and F. Ricci-Tersenghi, *private communication* (2012).
[75] E. Luijten and H. W. J. Blöte, Int. J. Mod. Phys. C **6**, 359 (1995).
[76] E. Luijten and H. W. J. Blöte, Phys. Rev. Lett. **76**, 1557 (1996).

[77] An alternative optimization can be realized by adopting cluster accelerating algorithms expressly designed for long-range systems.[75,76] We do not implement such algorithm in the present work.

[78] There is a more direct implication: $\langle \mathbf{m} \rangle = \mathbf{0}$, but this equation is also satisfied in presence of spontaneous magnetization, because of the equi-probability of the angle of the magnetized state.